electronics

MDPI

Article

Solar-Tracker Diffuse-Response Algorithm for Balancing Energy Gain and Mechanical Wear in Photovoltaic Systems

Riccardo Adinolfi Borea [1,*], Silvana Ovaitt [2], Vincenzo Cirimele [3,*], Mattia Ricco [3] and Giosuè Maugeri [1]

[1] RSE—Ricerca sul Sistema Energetico SpA, 20134 Milan, Italy; giosue.maugeri@rse-web.it
[2] NLR—National Laboratory of the Rockies, Golden, CO 80401, USA; silvana.ovaitt@nrel.gov
[3] Department of Electrical, Electronic, and Information Engineering, University of Bologna, 40136 Bologna, Italy; mattia.ricco@unibo.it
* Correspondence: adinolfi@rse-web.it (R.A.B.); vincenzo.cirimele@unibo.it (V.C.)

Abstract

Single-axis solar tracking maximizes photovoltaic energy production under clear-sky conditions; however, its effectiveness decreases under cloudy and overcast skies, where diffuse irradiance dominates and the optimal module orientation changes. Conventional tracking algorithms either neglect sky conditions or rely on simplified diffuse-response strategies that may trigger frequent tracker repositioning under variable cloud cover, leading to increased mechanical wear with marginal energy gains. This work proposes an enhanced diffuse-response tracking algorithm that explicitly accounts for both the intensity and temporal persistence of cloudiness. By requiring overcast conditions to persist for a minimum duration before reorienting the tracker to a diffuse-stow position, the proposed approach reduces unnecessary movements while preserving the benefits of diffuse-response operation. The algorithm is evaluated through numerical simulations based on historical meteorological data and validated using field measurements on monofacial and bifacial photovoltaic strings. The results show that the proposed strategy reduces excess tracker movement from 114% to 0.16% while maintaining nearly the same energy yield. Compared to a conventional diffuse-response algorithm, the associated energy reduction is minimal (≈0.17%) relative to the ≈0.37% yield gain observed at the studied location. These findings demonstrate that incorporating cloudiness duration enables a practical compromise between energy performance and tracker durability, particularly for monofacial photovoltaic systems.

Keywords: bifacial modules; tracking strategy; experimental validation; power maximization; energy yield

Check for updates

Academic Editors: Yiannis Katsigiannis and Konstantinos Blazakis

Received: 31 December 2025
Revised: 26 January 2026
Accepted: 28 January 2026
Published: 29 January 2026

Copyright: © 2026 by the authors. Licensee MDPI, Basel, Switzerland. This article is an open access article distributed under the terms and conditions of the Creative Commons Attribution (CC BY) license.

1. Introduction

The increasing availability of photovoltaic (PV) modules with higher power density and lower costs has accelerated the deployment of utility-scale PV systems. To further improve energy yield and plant profitability, these installations are commonly equipped with tracking systems that continuously adjust module orientation throughout the day. As a result, more than 90% of utility-scale PV projects in the United States now employ single-axis trackers [1].

The primary objective of a tracker control algorithm is to maximize the irradiance incident on the front surface of the PV module by tracking the Sun's position, often combined with back-tracking strategies to mitigate row-to-row shading [2]. Most commercial tracking algorithms, however, do not explicitly account for sky conditions. Experimental

and modeling studies have shown that cloud cover significantly affects the directionality of solar radiation and, consequently, the optimal module orientation [3]. Under clear-sky conditions, direct irradiance dominates, and solar tracking maximizes energy production. Under fully overcast conditions, the direct component vanishes, and a horizontal orientation (0°, commonly referred to as the diffuse-stow position) maximizes the collection of diffuse irradiance [4].

Between these two extremes, partially cloudy conditions may still exhibit a non-negligible direct component, even when diffuse irradiance is dominant. In such cases, the optimal orientation is not necessarily horizontal, but depends on the relative contributions of direct and diffuse radiation. Modeling studies by Pelaez et al. [3] and Anderson et al. [5] showed that orientation angles associated with different cloud-cover levels can outperform standard tracking, increasing energy yield by 0.1–0.8%, depending on local climatic conditions. An expanded analysis by Rodríguez-Gallegos et al. [6], which accounted for latitude and ground albedo, further demonstrated that discriminating between different cloud conditions when selecting the optimal orientation can improve insolation gain by up to 2%.

Despite these potential benefits, implementing such detailed orientation optimization in commercial trackers remains challenging. Accurate determination of the optimal angle would require high-resolution information on sky radiance distribution, as well as additional sensing and computational resources. For example, approaches based on rotating all-sky imagers that measure hemispherical irradiance at minute-scale resolution have been proposed, but their complexity limits large-scale deployment [7]. Consequently, most commercial solutions adopt simplified diffuse-response algorithms, which set the module to the diffuse-stow position whenever cloudiness exceeds a predefined threshold, without explicitly considering sky distribution.

A key limitation of diffuse-response algorithms is their sensitivity to short-term variability in cloud cover. Rapid fluctuations can trigger frequent tracker repositioning, leading to excessive mechanical movement. This increased activity accelerates component wear and raises the likelihood of mechanical failures [8]. To mitigate these effects, commercial controllers typically integrate signal-processing techniques such as time-averaging filters, hysteresis bands, and debounce logic. Time-averaging filters smooth the irradiance signal by calculating a moving average over a sliding window, effectively suppressing high-frequency noise from transient cloud movements [9]. Hysteresis bands establish different activation and deactivation thresholds to set modules to the diffuse-stow position, preventing rapid oscillation of actuators when the irradiance fluctuates near a single decision point [10]. Debouncing strategies impose a mandatory residence time, requiring a signal to remain above or below a threshold for a short, predefined duration before an action is triggered [11]. While these techniques are effective at suppressing noise and rapid oscillations, they operate implicitly on the measurement signal and do not explicitly encode the persistence of a given sky condition. As a result, tracker repositioning may still occur during transient but sustained cloudy periods, depending on the selected filter length, hysteresis width, or debounce time.

Field experience indicates that tracker-related issues represent a significant fraction of operational challenges in utility-scale PV plants. In particular, tracker faults account for approximately 11% of all service requests, ranking among the top three causes after inverters (≈60%) and modules (≈18%) [12]. Moreover, tracker-related tickets typically require longer resolution times than other components, with an average duration of approximately 14 days. Of this time, nearly 50% is associated with on-site service activities and an additional 30% with component repair or replacement, highlighting the operational burden associated with tracker failures. Reliability analyses based on large-scale field data further

highlight the vulnerability of tracker components to frequent actuation. Using statistics from Sandia's Photovoltaic Reliability, Operations & Maintenance (PVROM) database, Gunda et al. [13] reported mean times to failure of approximately 1.1 years for tracker motors and 1.7 years for tracker bearings. In [14], the authors analyzed tracker availability in utility-scale PV plants and found that tracker-related failures can lead to power losses of up to 11–12%, with an average tracker uptime of approximately 85%, where the uptime represents the percentage of operational time during which the tracker functions as intended. These relatively short lifetimes, compared to other balance-of-system components, indicate that excessive or unnecessary tracker movement can significantly increase maintenance requirements and operational downtime.

Within this context, the objective of this work is to refine diffuse-response tracking by introducing an explicit temporal persistence criterion for overcast conditions. In addition to identifying an appropriate cloudiness threshold, the proposed approach requires overcast conditions to persist for a minimum duration before entering the diffuse-stow position. Unlike conventional time-averaging, hysteresis, and debouncing logic—which mitigate excessive actuation by implicitly conditioning the irradiance signal over predefined windows or thresholds—the proposed duration threshold explicitly encodes the persistence of a given sky condition. The threshold is defined over longer, meteorologically meaningful intervals and is directly designed to balance energy yield against mechanical wear. By integrating the temporal persistence of cloudiness into the control logic, the proposed approach aims to reduce unnecessary tracker repositioning while preserving the energy gains associated with diffuse-response strategies.

The algorithm is evaluated through numerical simulations and validated using field measurements on both monofacial and bifacial PV systems, enabling a quantitative assessment of the trade-off between energy yield and tracker wear.

The remainder of the paper is organized as follows. Section 2 outlines the methodology for modeling PV performance, defining diffuse-response tracking algorithms, and evaluating trade-offs between energy yield and mechanical wear. Results from numerical simulations and field validations are detailed in Section 3, showcasing the algorithm's effectiveness for monofacial and bifacial systems. Section 4 concludes by summarizing findings, implications for practical implementation, and future perspectives for enhancing tracking strategies in diverse climatic contexts.

2. Methodology

This section describes the modeling framework used to simulate PV module performance, the formulation of the diffuse-response tracking algorithm, and the metrics adopted to evaluate energy yield and tracker movement.

PV module performance is simulated using the Python library PVlib [15]. Optical effects are modeled through the infinite-sheds approach [16], thermal behavior is described using the Sandia thermal model [17], and electrical output is computed with the PVWatts model [18]. This modeling chain is widely adopted in the literature and is applied here to both monofacial and bifacial modules, following established practices [19]. The primary specifications of the PV module are detailed in Table 1. For the bifacial technology, the model introduces a bifaciality factor of 0.7, whereas this value is null for the monofacial case. All other parameters are kept identical across both configurations to isolate the effect of the rear-side irradiance and prevent secondary variables from confounding the comparative analysis.

Table 1. PV module and system's main characteristics.

Parameter	Value
output power thermal coeff.	$-0.4\%/^{\circ}C$
nameplate output power	350 W
thermal coeff. a	-3.47
thermal coeff. b	-0.0594
thermal coeff. ΔT	3
bifaciality factor	0 or 0.7
albedo	0.20
module length	2 m
module's height	1.5 m
tracker limit angle	50°
ground coverage ratio	0.3

Sky conditions are characterized using the ratio of direct normal irradiance (DNI) to diffuse horizontal irradiance (DHI). High DNI/DHI values correspond to clear-sky conditions dominated by direct irradiance, whereas low values indicate overcast conditions in which diffuse irradiance prevails. This ratio is commonly used in diffuse-response algorithms because it captures the directional nature of solar radiation while remaining independent of absolute irradiance levels [20].

To generate a controlled range of sky-condition scenarios, a clear-sky reference case is defined using the spring equinox in Golden, CO [21]. A scaling factor ζ in the [0, 1] range is applied to DNI, while the DHI profile is kept unchanged, as expressed in Equation (1):

$$\begin{cases} DNI_i = \zeta \, DNI_{cs} \\ DHI_i = DHI_{cs} \end{cases} \tag{1}$$

$\zeta = 0$ represents a fully overcast sky, and $\zeta = 1$ a clear sky. The subscript i denotes the considered scenario, and cs the clear-sky reference. Although real atmospheric conditions often couple reductions in DNI with increases in DHI, diffuse-response strategies are typically evaluated on the basis of the DNI/DHI ratio rather than the absolute values of each component. This simplification allows the creation of a dataset used solely to identify when modules should be set to the diffuse-stow position, consistent with previous studies [20]. Subsequent diffuse-response validation is carried out with real weather data.

The diffuse-response algorithm is derived by simulating the output power of the PV module across the tracker's angular range under different sky conditions. This analysis is used to correlate the optimal orientation with the DNI/DHI ratios corresponding to different cloudiness levels, and determine the conditions under which a horizontal orientation (i.e., diffuse-stow position at 0°) becomes preferable. For commercial applications, this evaluation is reduced to introducing a cloudiness threshold, C_1: when the evaluated sky condition exceeds this threshold, the tracker is set to the diffuse-stow position. Otherwise, it follows the standard solar-tracking strategy. This implementation is represented by the blue box depicted in Figure 1.

The proposed algorithm extends this conventional logic by introducing an additional parameter (C_2), which allows for taking into account a minimum duration for which overcast conditions must persist before the tracker is oriented at the diffuse-stow orientation. In this formulation, short-lived fluctuations in DNI/DHI do not immediately trigger tracker movement. By requiring temporal persistence of cloudy conditions, the algorithm aims to limit unnecessary repositioning under rapidly changing skies. The introduction of this new threshold parameter over the standard tracking is represented by the orange box depicted in Figure 1.

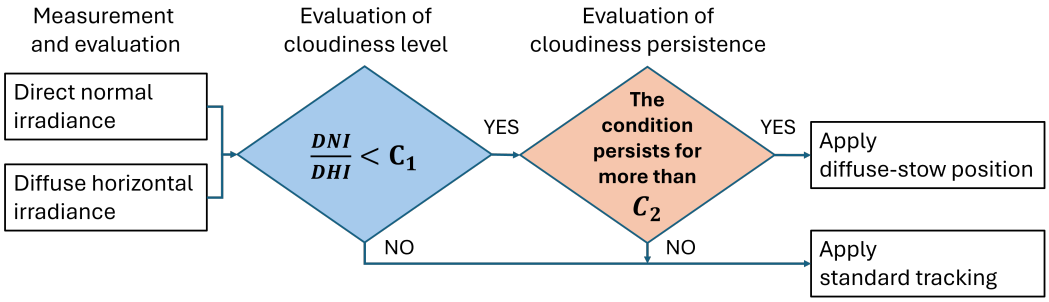

Figure 1. The blue decision block mirrors the operation of a commercial solution that only evaluates the cloudiness level against the C_1 threshold value. The proposed algorithm considers the addition of the orange block, which takes into account the duration of the cloudiness period by comparing it to the C_2 threshold value.

The performance of the diffuse-response algorithm is evaluated by comparison with standard tracking in terms of both annual energy yield and cumulative tracker movement. Energy yield is calculated as the sum of the electrical energy produced at each time step, while tracker movement is quantified as the cumulative angular displacement executed by the tracker. The relative annual energy gain ΔE and the relative increase in tracker movement ΔM are defined as follows:

$$\Delta E = 100\left(\frac{\sum_k e_{dr,k}}{\sum_k e_{reg,k}} - 1\right) \tag{2}$$

and

$$\Delta M = 100\left(\frac{\sum_k m_{dr,k}}{\sum_k m_{reg,k}} - 1\right), \tag{3}$$

where e and m denote, respectively, the energy produced and the angular movement at time step k, and the subscripts dr and reg refer to diffuse-response and regular tracking.

Validation is carried out using field data, while numerical simulation of the yearly potential energy gains is performed using historical data. The historical weather data is retrieved from the National Solar Radiation Database [22] for the location of Golden, and contains DHI, DNI, DNI under clear-sky conditions, air temperature, wind speed, and the solar zenith and azimuth angles, with a temporal resolution of 5 min for the year 2022. Field data are obtained from the National Laboratory of the Rockies (NLR) Bifacial Experimental Single-Axis Tracking Field (BEST field), shown in Figure 2, located at the NLR's South Table Mountain Campus in Golden. The facility consists of ten PV module rows equipped with independently controlled single-axis trackers [23]. Measurements are initially taken at 1-min intervals and subsequently downsampled to a 10-min average frequency.

Figure 2. Picture of the PV field during an overcast day (7th of March 2025). It can be seen how some rows are fixed at 0° while the others are tracking.

The experiments aimed to confirm the optimal C_1 threshold that is firstly found via modeling. Two strings were utilized: one operating in standard tracking mode and the other fixed in the diffuse-stow position. Both rows were located away from the array edges to ensure similar ground-reflected irradiance, wind, and air temperature conditions. Experiments are first carried out using monofacial modules and subsequently repeated with bifacial modules. The comparison between strings is performed using the normalized power gain GP, defined as

$$GP = \frac{P_0}{P_{\text{reg}}} - 1\,, \tag{4}$$

where P_0 and P_{reg} represent the normalized output power of the string in the diffuse-stow position and under standard tracking, respectively.

3. Results

This section presents the results obtained from numerical simulations and field measurements. First, the influence of sky conditions on the optimal tracker orientation is investigated through simulations. The diffuse-response algorithm is then assessed using historical weather data, followed by experimental validation using field measurements on monofacial and bifacial PV strings.

3.1. Influence of Sky Conditions on Optimal Orientation

Numerical simulations are first used to investigate how the optimal tracker orientation varies with sky conditions at different times of day and DNI/DHI values. Figure 3a shows the orientation that maximizes output power as a function of the DNI/DHI ratio and hour of the day. As DNI/DHI decreases, the optimal orientation progressively shifts toward 0°, regardless of the time of day. This behavior becomes particularly evident for DNI/DHI values below approximately 1, where the influence of the Sun's position diminishes as the radiation field becomes increasingly diffuse.

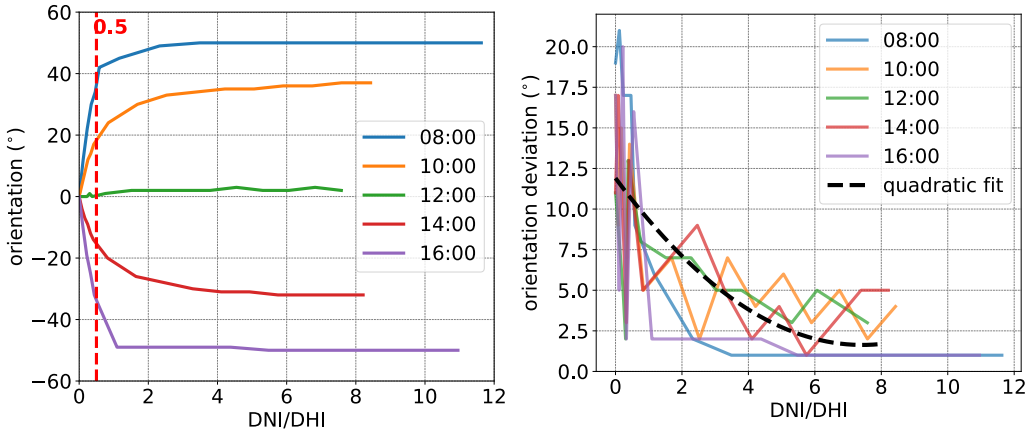

(**a**) (**b**)

Figure 3. Influence of DNI/DHI and time of the day on the best orientation of a monofacial PV module. (**a**) Best orientation for different cloudiness levels and hours of the day. The vertical dashed red line marks $DNI/DHI = 0.5$. (**b**) Deviation from the best orientation that does not affect the module's output power, for different DNI/DHI values and hours of the day. At $DNI/DHI \sim 0$, the deviation approaches values above 10°, showing low relevance of the module's orientation.

To further assess the sensitivity of module output to orientation under different sky conditions, Figure 3b shows the angular deviation from the optimal orientation that results in negligible changes in output power. For very low DNI/DHI values, the allowable deviation increases significantly, reaching values above 10°. For instance, when DNI/DHI

approaches zero, the module can be oriented within a wide angular range around 0° without appreciable power losses. This indicates that, under strongly diffuse conditions, precise orientation control becomes less critical.

This behavior is partially influenced by the adopted simulation framework. With constant DHI and very low DNI/DHI ratios, overall irradiance levels are low, and variations in orientation have a limited impact on absolute power output. As an example, at noon with $\zeta = 0.02$, the simulated output power varies only between approximately 36 and 43 W/m^2 over the tracker's full range of motion. While this simplification does not capture the full complexity of atmospheric interactions—specifically, the inverse correlation between DNI reduction and DHI increase—it remains sufficient for characterizing the relative trends of optimal orientation. As demonstrated by [20], the definition of an effective diffuse-response strategy depends primarily on the DNI/DHI ratio rather than absolute irradiance values, rendering this approach a reliable proxy only for determining optimal orientation, not predicting output power.

Based on these results, the diffuse-response algorithm is configured to set the module orientation to 0° when the DNI/DHI ratio falls below a threshold value of $C_1 = 0.5$. Although the strictly optimal orientation approaches 0° only as DNI/DHI tends toward zero, the reduced sensitivity to orientation at low ratios justifies the use of a single horizontal position for all conditions with $DNI/DHI < 0.5$. For higher ratios, the algorithm defaults to standard tracking. This threshold is first evaluated using historical weather data and subsequently validated through field measurements.

3.2. Algorithm Assessment Using Historical Weather Data

The diffuse-response algorithm is subsequently evaluated using historical meteorological data for Golden, CO. Figure 4a summarizes the monthly values of the relative energy gain (ΔE) and relative tracker movement (ΔM) obtained when the algorithm is applied without any minimum cloudiness duration (i.e. $C_2 = 0$). On an annual basis, the algorithm yields an energy gain $\Delta E = 0.37\%$, with higher monthly gains occurring during winter, when overcast conditions are more frequent.

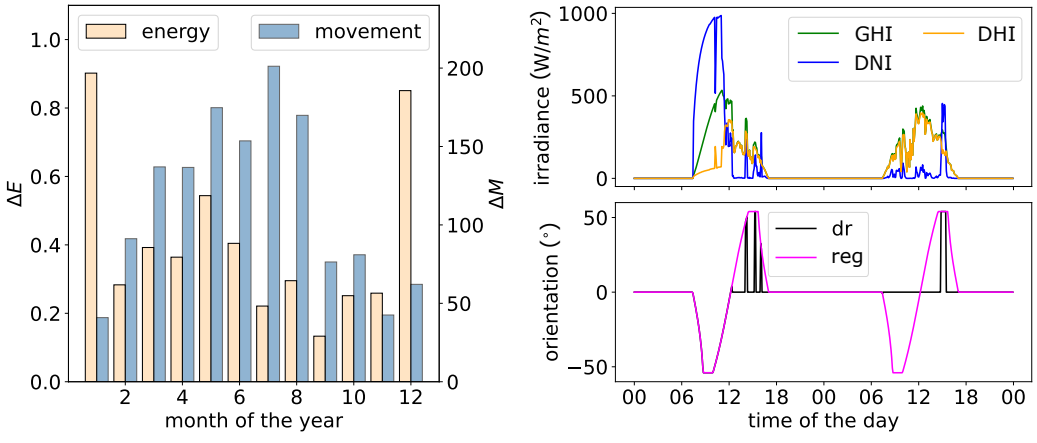

(**a**) (**b**)

Figure 4. Comparison of diffuse-response and standard tracking. (**a**) Monthly ΔE and ΔM. While ΔE is greater in winter, ΔM is greater in summer, both due to weather variability. (**b**) Example of the orientation provided by diffuse-response (dr) and standard tracking (reg) during two partially overcast days. ΔM is strongly affected by sky conditions' variability.

In contrast, tracker movement increases substantially, reaching a yearly value of $\Delta M = 114.24\%$. The increase is most pronounced during summer months, when short and intermittent cloudy periods are more common. This behavior is illustrated in Figure 4b,

which compares tracker orientations under diffuse-response and standard tracking during two partially overcast days. During the first afternoon, rapid fluctuations in DNI/DHI lead to repeated repositioning under diffuse-response tracking, resulting in additional movement. During the second morning, persistent overcast conditions reduced movement relative to standard tracking, highlighting the strong dependence of ΔM on cloud variability.

To mitigate excessive movement while preserving energy gains, the modified diffuse-response algorithm is tested with different values of the minimum cloudiness duration threshold C_2. Figure 5a shows the annual values of ΔE and ΔM as a function of C_2. Increasing the required persistence of overcast conditions reduces both energy gain and tracker movement. For example, increasing C_2 from 5 to 65 min reduces ΔE from 0.37% to 0.17%, while ΔM decreases from 114.24% to -4.97%. A minimum cloudiness duration threshold of approximately 50 min provides a favorable compromise between energy yield and tracker movement. For this value, the algorithm achieves $\Delta E = 0.20\%$ while reducing additional tracker movement to $\Delta M = 0.16\%$, effectively eliminating excess actuation relative to standard tracking. To characterize the meteorological variability of Golden and the number of unexploited events, Figure 5b illustrates the distribution of overcast event durations (where $DNI/DHI < 0.5$). The data indicate that Golden is a predominantly clear-sky location characterized by transient cloud cover. Consequently, these results may not be fully representative of climates with more persistent or stable overcast conditions.

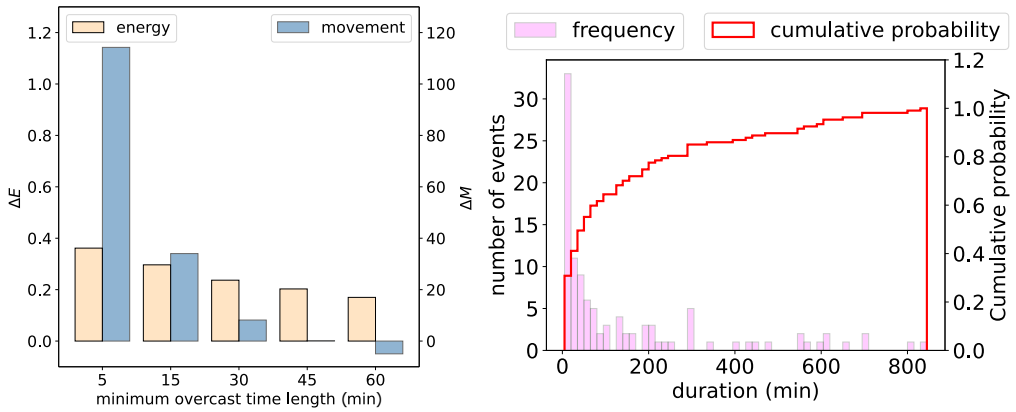

(**a**) (**b**)

Figure 5. Implementation of diffuse-response tracking algorithm using real weather data for the city of Golden: (**a**) Variation in ΔE and ΔM using different minimum cloudiness period lengths to set the module flat. Considering a cloudiness minimum duration of 45 min permits $\Delta E = 0.20\%$ and $\Delta M = 0.16\%$. (**b**) Distribution of event durations during which DNI/DHI falls below 0.5. The red line depicts the cumulative probability distribution.

To assess the algorithm's performance under contrasting meteorological conditions, the analysis is extended to Milan, Italy—a region characterized by lower average wind speeds and more persistent cloud cover. While the Golden dataset permitted a 5-min resolution, historical irradiance and temperature data for Milan were restricted to a 15-min time resolution due to data availability. Figure 6a presents a comparative performance analysis using the metrics established for the Golden site. Notably, the algorithm yields more pronounced improvements; a threshold of $C_2 = 15$ min results in an energy gain of $\Delta E = 0.45\%$. Furthermore, Milan exhibits consistently lower ΔM than Golden for equivalent C_2 values. A threshold of $C_2 = 30$ min is sufficient to achieve $\Delta E = 0.30\%$ while obtaining $\Delta M = -0.20\%$. As illustrated in Figure 6b, the overcast duration distribution in Milan differs substantially from that of Golden, confirming that the C_2 parameter must be specifically tuned to local sky conditions to ensure optimal implementation.

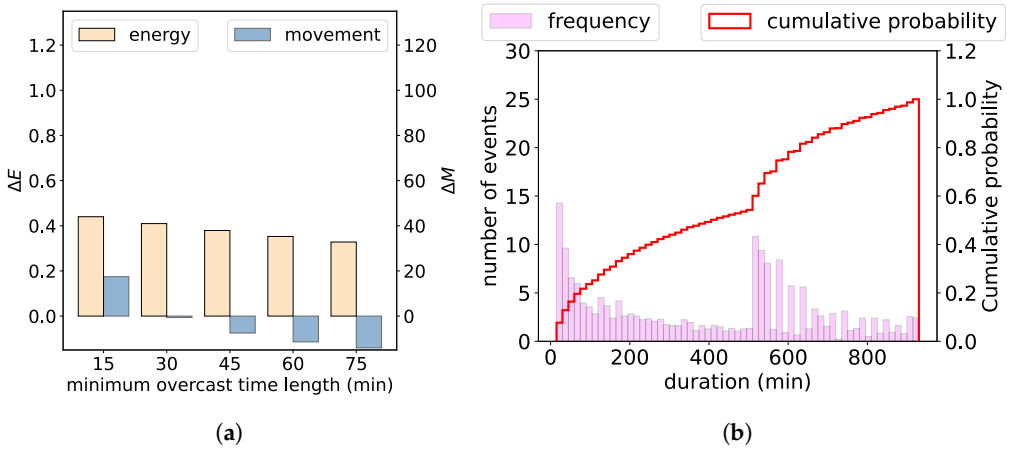

(**a**) (**b**)

Figure 6. Implementation of diffuse-response tracking algorithm using real weather data for the city of Milan: (**a**) Variation in ΔE and ΔM using different minimum cloudiness period lengths to set the module flat. Considering a cloudiness minimum duration of 30 min permits $\Delta E = 0.30\%$ and $\Delta M = -0.20\%$. (**b**) Distribution of event durations during which DNI/DHI falls below 0.5. The red line depicts the cumulative probability distribution.

The selected value for C_2 is consistent with the capabilities of current nowcasting techniques in forecasting short-term irradiance variability [24,25]. The results indicate that a yield increase of 0.2–0.4% translates to an equal LCOE reduction relative to the baseline, neglecting changes in O&M cost due to tracker movement and nowcasting solutions that might be required for implementation of these strategies, which are now increasingly integrated into utility-scale PV infrastructure [24].

3.3. Validation with Field Data

The value of C_1, identified through modeling, is validated using field measurements collected during March 2025. The overall accuracy from the highly instrumented research site is <3%, including environmental variability and irradiance sensor stability, with power measurement uncertainty under 1%. Figure 7 illustrates the deviations between modeled and measured output power for strings operating under normal conditions and those fixed at 0° (monofacial and bifacial). Modeled versus measured measurements yielded an MBD and RMSE of 4–6% and 12–14%, respectively.

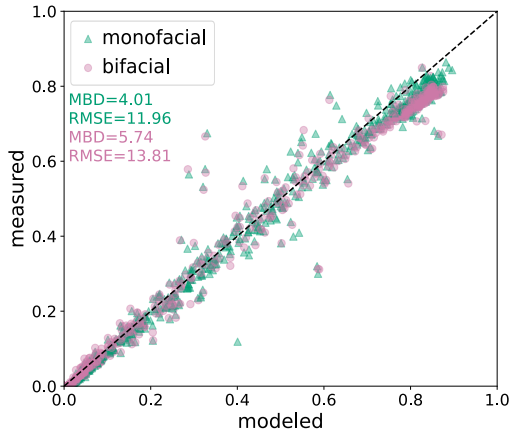

Figure 7. Parity plot of modeled versus measured output power for the monofacial and bifacial strings, operating as expected and fixed at 0°.

Figure 8 shows the measured irradiance conditions, the corresponding DNI/DHI ratio, and the calculated normalized power gain GP for two monofacial strings and, separately, for two bifacial strings. For the monofacial case, periods with positive power gain (i.e., $GP > 0.01$) consistently coincide with DNI/DHI values below 0.5. This indicates that, under cloudy conditions, the string fixed at the diffuse-stow position systematically outperforms the string operating under standard tracking. The experimental results, therefore, confirm the suitability of the selected value for C_1.

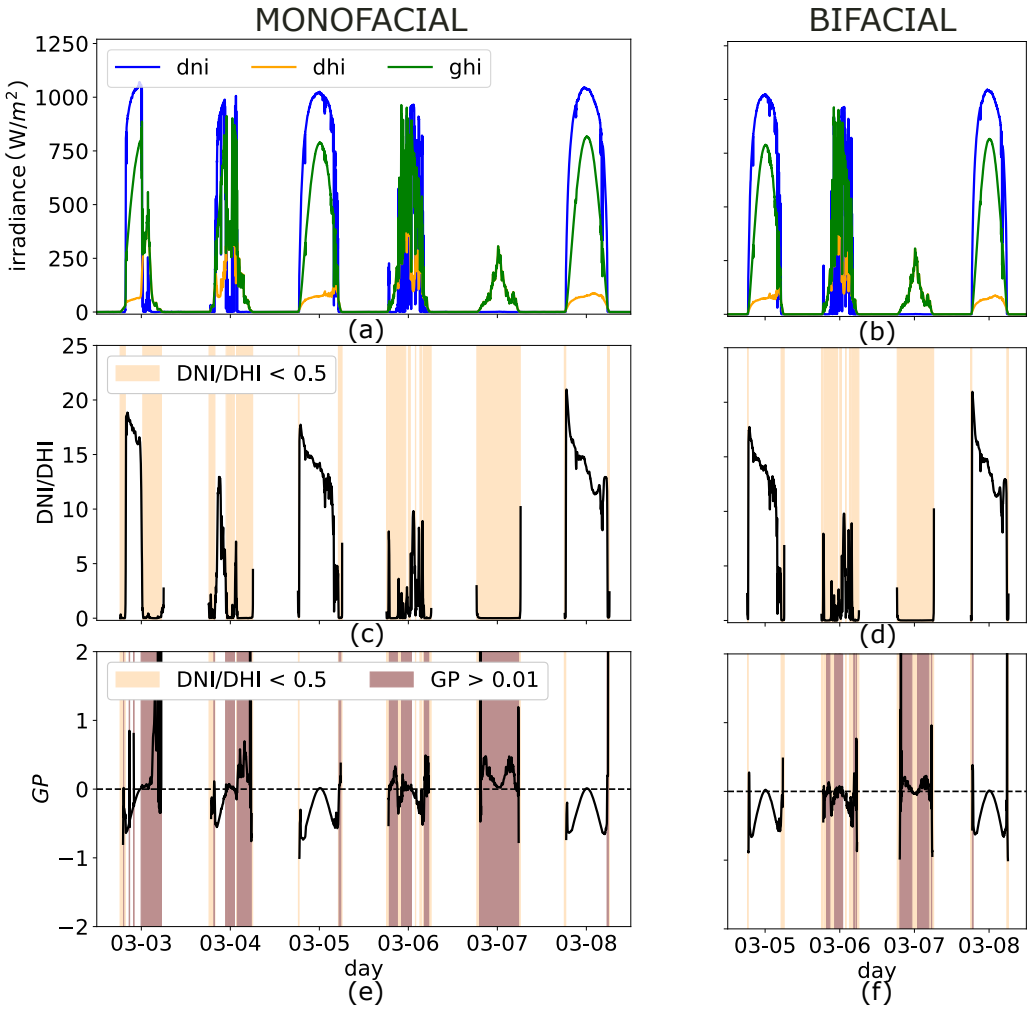

Figure 8. The top Experimental results from field data. The left column (**a**,**c**,**e**) evaluates the performance of the monofacial string configuration, while the right column (**b**,**d**,**f**) illustrates the bifacial string comparison. (**a**,**b**) show the irradiance profiles of the days under consideration. (**c**,**d**) show the calculated ratio DNI/DHI, with colored sections marking intervals where the ratio falls below 0.5. (**e**,**f**) show the GP, with brown sections highlighting sections where GP is positive.

In contrast, the bifacial comparison does not exhibit the same consistent behavior. Periods with $DNI/DHI < 0.5$ do not always correspond to positive power gains for the diffuse-stow configuration. This qualitative analysis suggests that additional factors influence the performance of bifacial modules under diffuse-response operation. This behavior is quantified via modeling in Figure 9, which shows the variance in incident irradiance resulting from the transition to a diffuse-stow strategy. Specifically, the figure illustrates the modeled irradiance gain achieved by adopting a horizontal stow position relative to standard tracking when $DNI/DHI < 0.5$. These results are generated using the aforementioned simulation framework, for the location of Golden, and employing the same 5-min weather data retrieved from NSRDB that was used for the yearly assessment. It is

possible to note that, while the diffuse-stow orientation increases front-side irradiance under cloudy conditions, it simultaneously reduces rear-side irradiance. For monofacial modules, rear irradiance contributes only indirectly through thermal effects, making this reduction beneficial. For bifacial modules, instead, the reduction in rear-side irradiance offsets or entirely counteracts the gains captured on the front surface. As a result, the net benefit of diffuse-response strategies under low-DNI/DHI conditions is reduced, consistent with field observations.

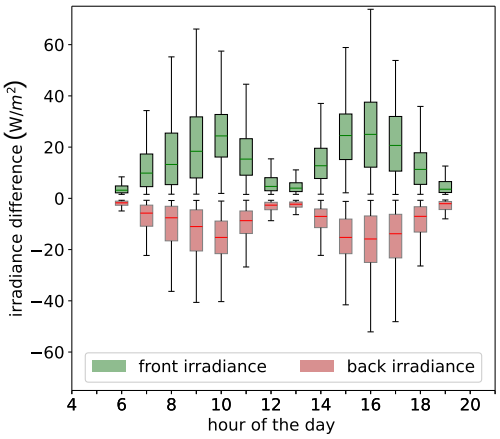

Figure 9. Incident irradiance difference when using diffuse-response instead of standard tracking, depending on the time of the day, along the whole solar year. While the front incident irradiance increases in the diffuse-stow position, the back incident irradiance decreases.

4. Conclusions

This work investigates the trade-off between energy yield and mechanical wear in single-axis tracking systems by refining diffuse-response tracking strategies under cloudy conditions. By characterizing sky conditions through the DNI/DHI ratio, the study identifies the conditions under which orienting PV modules in a diffuse-stow position improves performance, while also quantifying the impact of frequent repositioning on tracker movement.

Numerical simulations show that, when the DNI/DHI ratio falls below 0.5, the optimal module orientation shifts toward 0°, and the sensitivity of power output to orientation is significantly reduced. A diffuse-response strategy based solely on a cloudiness threshold yields a modest annual energy gain ($\Delta E = 0.37\%$) but results in a substantial increase in tracker movement ($\Delta M = 114.24\%$). Introducing a minimum cloudiness duration threshold before entering the diffuse-stow position effectively mitigates this drawback. For a minimum duration of approximately 45 min, excess tracker movement is reduced to negligible levels ($\Delta M = 0.16\%$), while maintaining a positive energy gain ($\Delta E = 0.20\%$). Considering locations with different weather conditions leads to different results, as for the city of Milan, where a C_2 of 30 min allows for $\Delta E = 0.30\%$ and $\Delta M = -0.20\%$. Preliminary results indicate that a yield increase of 0.2% – 0.4% translates to an equal LCOE reduction relative to the baseline.

Field measurements confirm the validity of the selected DNI/DHI threshold for monofacial PV modules. Under cloudy conditions, monofacial strings fixed at the diffuse-stow position consistently outperform those operating under standard tracking. In contrast, the same strategy does not provide consistent benefits for bifacial modules, as gains in front-side irradiance are partially offset by reductions in rear-side irradiance. These results demonstrate that the effectiveness of diffuse-response algorithms is reduced for bifacial modules when rear-side irradiance is explicitly accounted for. In this case, rear-side generation partially offsets the benefits of diffuse-stow operation. Further optimization

of gains would likely require added control complexity to account for spatially varying diffuse light and orientation-dependent rear-side light distributions.

Future work should focus on field-based validation of diffuse-response control under real operating conditions, particularly to better understand its influence on tracker motion frequency, mechanical wear, and maintenance requirements. Since this is an initial field study, more field measurements are required to solidify the trends seen here. Improved characterization of these operational effects, alongside energy-yield impacts, would enable a more complete assessment of the long-term reliability and LCOE implications of advanced tracker control strategies.

Overall, the proposed algorithm demonstrates that incorporating cloudiness duration into diffuse-response tracking enables a practical compromise between energy performance and tracker durability. The approach can be implemented with limited additional complexity and does not require high-resolution sky imaging or advanced sensing. While particularly well suited for monofacial PV systems, further refinement is required to extend its effectiveness to bifacial applications, potentially through adaptive thresholds or irradiance-based weighting of front and rear contributions.

Author Contributions: Conceptualization, Methodology, Validation, Writing—Original Draft Preparation, R.A.B. and S.O.; Methodology, Writing—Review and Editing, Supervision, V.C.; Resources, G.M. and S.O.; Writing—Review and Editing, M.R. All authors have read and agreed to the published version of the manuscript.

Funding: This work has been supported by Ricerca per il Sistema Energetico Spa (RSE) through the Fondo di Ricerca per il Sistema Elettrico (RdS) within the framework of the Triennial Plan 2022–2024 (DM MITE n. 337, of 15.09.2022) and the RdS 1.1 project "High-Efficiency Photovoltaics", supported by the Alma Mater Studiorum—Universita' di Bologna through the National Doctoral Program in "Photovoltaics" for the XXVIII cycle, as per article 3, paragraph 2 of DM 226/2021.

This work was authored in part by the National Laboratory of the Rockies for the U.S. Department of Energy (DOE), operated under Contract No. DE-AC36-08GO28308. Funding was provided by the U.S. DOE of Critical Minerals and Energy Innovation Solar Energy Technologies Office, Agreement 52799. The views expressed in the article do not necessarily represent the views of the DOE or the U.S. Government. By accepting the article for publication, the publisher acknowledges that the U.S. Government retains a nonexclusive, paid-up, irrevocable, worldwide license to publish or reproduce the published form of this work, or allow others to do so, for U.S. Government purposes.

Data Availability Statement: The field data supporting the findings of this study are publicly available online on the Duramat DataHub and upon request. Historical weather data are available from the National Solar Radiation Database (NSRDB). PVLib is available as an open-source Python package for the calculation of module performance.

Conflicts of Interest: The authors declare that they have no known competing financial interests or personal relationships that could have appeared to influence the work reported in this paper.

References

1. Masson, G.; De l'Epine, M.; Kaizuka, I. *Trends in PV Applications*; Report IEA PVPS T1-43:2024; IEA-PVPS: Paris, France, 2024. https://doi.org/10.69766/JNEW6916.
2. Lorenzo, E.; Narvarte, L.; Munoz, J. Tracking and back-tracking. *Prog. Photovolt. Res. Appl.* **2011**, *19*, 747–753. https://doi.org/10.1002/pip.1085.
3. Pelaez, S.A.; Deline, C.; Greenberg, P.; Stein, J.S.; Kostuk, R.K. Model and validation of single-axis tracking with bifacial PV. *IEEE J. Photovoltaics* **2019**, *9*, 715–721. https://doi.org/10.1109/JPHOTOV.2019.2892872.
4. Kelly, N.A.; Gibson, T.L. Increasing the solar photovoltaic energy capture on sunny and cloudy days. *Sol. Energy* **2011**, *85*, 111–125. https://doi.org/10.1016/j.solener.2010.10.015.

5. Anderson, K.; Aneja, S. Single-axis tracker control optimization potential for the contiguous United States. In Proceedings of the 2022 IEEE 49th Photovoltaics Specialists Conference (PVSC), Philadelphia, PA, USA, 5–10 June 2022; pp. 1–6. https://doi.org/10.1109/PVSC48317.2022.9938629.
6. Rodriguez-Gallegos, C.D.; Gandhi, O.; Panda, S.K.; Reindl, T. On the PV tracker performance: Tracking the sun versus tracking the best orientation. *IEEE J. Photovoltaics* **2020**, *10*, 1474–1480. https://doi.org/10.1109/JPHOTOV.2020.3006994.
7. Zapotocky, C.; Riley, D. *Concurrent Sky Images, Hemispherical Irradiance Profiles, and Weather Data for Albuquerque and Eugene*; Sandia National Laboratory: Albuquerque, NM, USA, 2025. Available online: https://data.openei.org/submissions/8414 (accessed on 1 December 2025).
8. Enbar, N.E.; Weng, D.W.; Klise, G.T. *Budgeting for Solar PV Plant Operations & Maintenance: Practices and Pricing*; Sandia National Laboratory: Albuquerque, NM, USA, 2016. https://doi.org/10.2172/1237001.
9. Flores-Hernández, D.A.; Islas-Estrada, L.R.; Palomino-Resendiz, S.I. A Novel Tracking Strategy Based on Real-Time Monitoring to Increase the Lifetime of Dual-Axis Solar Tracking Systems. *Appl. Sci.* **2024**, *14*, 8281. https://doi.org/10.3390/app14188281.
10. Mousazadeh, H.; Keyhani, A.; Javadi, A.; Mobli, H.; Abrinia, K.; Sharifi, A. A review of principle and sun-tracking methods for maximizing solar systems output. *Renew. Sustain. Energy Rev.* **2009**, *13*, 1800–1818. https://doi.org/10.1016/j.rser.2009.01.022.
11. Fuentes-Morales, R.F.; Diaz-Ponce, A.; Peña-Cruz, M.I.; Rodrigo, P.M.; Valentín-Coronado, L.M.; Martell-Chavez, F.; Pineda-Arellano, C.A. Control algorithms applied to active solar tracking systems: A review. *Sol. Energy* **2020**, *212*, 203–219. https://doi.org/10.1016/j.solener.2020.10.071.
12. Charity, N.V.; Faith, S.; Shinn, A. Extracting insight from unstructured solar text logs. In Proceedings of the Photovoltaic Reliability Workshop (PVRW), Lakewood, CO, USA, 27–29 February 2024. Available online: https://pvrw.nrel.gov/past-proceedings (accessed on 1 December 2025).
13. Gunda, T.; Homan, R. *Evaluation of Component Reliability in Photovoltaic Systems Using Field Failure Statistics*; Sandia National Laboratory: Albuquerque, NM, USA, 2020. https://doi.org/10.2172/1660804.
14. Chowdhury, G. Assessing Tracker Availability in Utility-Scale Solar Power Plants. In Proceedings of the PV Performance Modeling Collaborative (PVPMC) workshop, Rome, Italy, 13–15 May 2025. Available online: https://PVPMC.sandia.gov/workshops-and-pubs/workshops/2025-pvpmc-albuquerque/ (accessed on 1 December 2025).
15. Holmgren, W.F.; Hansen, C.W.; Mikofski, M.A. Pvlib python: A python package for modeling solar energy systems. *J. Open Source Softw.* **2018**, *3*, 884. https://doi.org/10.21105/joss.00884.
16. Mikofski, M.A.; Darawali, R.; Hamer, M.; Neubert, A.; Newmiller, J. Bifacial performance modeling in large arrays. In Proceedings of the 2019 IEEE 46th Photovoltaic Specialists Conference (PVSC), Chicago, IL, USA, 16–21 June 2019. https://doi.org/10.1109/PVSC40753.2019.8980572.
17. Oh, J.; Pavgi, A.; Tamizhmani, G. Determination of empirical coefficients and δt for Sandia thermal model: Dependence on backsheet type. In Proceedings of the 2018 IEEE 7th World Conference on Photovoltaic Energy Conversion (WCPEC), Waikoloa, HI, USA, 10–15 June 2018. https://doi.org/10.1109/PVSC.2018.8547779.
18. Dobos, A.P. *PVWatts Version 5 Manual*; National Renewable Energy Laboratory: Golden, CO, USA, 2014. https://doi.org/10.2172/1158421.
19. Adinolfi Borea, R.; Cirimele, V.; Lo Franco, F.; Maugeri, G.; Melino, F. Impact of environmental variables on tilt selection for energy yield maximization in bifacial photovoltaic modules. *Appl. Sci.* **2024**, *14*, 11497. https://doi.org/10.3390/app142411497.
20. McIntosh, K.; Abbott, M.; Sudbury, B. The Optimal Tilt Angle of Monofacial and Bifacial Modules on Single-Axis Trackers. *IEEE J. Photovoltaics* **2022**, *12*, 397–405. https://doi.org/10.1109/JPHOTOV.2021.3126115.
21. Ineichen, P. Validation of models that estimate the clear sky global and beam solar irradiance. *Sol. Energy* **2016**, *132*, 332–344. https://doi.org/10.1016/j.solener.2016.03.017.
22. National Solar Radiation Database. Available online: http://nsrdb.nrel.gov (accessed on 1 December 2025).
23. Duramat Datahub. Available online: https://datahub.duramat.org/dataset/best-field-data (accessed on 1 December 2025).
24. Lauret, P.; Alonso-Suárez, R.; e Silva, R.A.; Boland, J.; David, M.; Herzberg, W.; Salle, J.L.G.L.; Lorenz, E.; Visser, L.; van Sark, W.; et al. The added value of combining solar irradiance data and forecasts: A probabilistic benchmarking exercise. *Renew. Energy* **2024**, *237*, 121574. https://doi.org/10.1016/j.renene.2024.121574.
25. Luppi, C.; Tiburtini, F.M.; Lo Franco, F.; Cirimele, V.; Apicella, V.; Carambia, B.; Ricco, M. Gradient Boosting-Based Model for Photovoltaic Power Prediction Using Local and Satellite-Based Weather Data. In *ELECTRIMACS 2024. Selected Papers—Volume 2*; Springer: Cham, Switzerland, 2024.

Disclaimer/Publisher's Note: The statements, opinions and data contained in all publications are solely those of the individual author(s) and contributor(s) and not of MDPI and/or the editor(s). MDPI and/or the editor(s) disclaim responsibility for any injury to people or property resulting from any ideas, methods, instructions or products referred to in the content.